https://doi.org/10.18321/ectj1498

Effect of Pre-Oxidation of Electrospun Polyvinylpyrrolidone-Derived Co_xP/C Composite Nanofibers on their Electrochemical Performance as Anode in Lithium-Ion Batteries

S. Berikbaikyzy[1,2], Y. Sagynbay[1], G. Turarova[1], I. Taniguchi[3], Zh. Bakenov[1,2], A. Belgibayeva[1,2]*

[1]National Laboratory Astana, Nazarbayev University, Kabanbay Batyr Ave. 53, Astana, Kazakhstan
[2]School of Engineering and Digital Sciences, Nazarbayev University, Kabanbay Batyr Ave. 53, Astana, Kazakhstan
[3]Department of Chemical Science and Engineering, Tokyo Institute of Technology, Tokyo 152-8552, Japan

Article info

Received:
20 December 2022

Received in revised form:
16 March 2023

Accepted:
3 April 2023

Keywords:
Lithium-ion batteries,
Electrospinning,
Conversion-based anodes,
Phosphides, Pre-oxidation.

Abstract

This research studies the effect of pre-oxidation on physical and electrochemical properties of electrospun polyvinylpyrrolidone (PVP)-derived carbon composites of cobalt phosphides by comparing carbonized non-pre-oxidized (NPO) and pre-oxidized (PO) samples used as anode materials for lithium-ion batteries. The X-Ray diffraction (XRD) patterns revealed the formation of CoP and Co_2P in both samples while presence of amorphous cobalt metaphosphate for NPO and cobalt phosphate for PO was determined by X-ray photoelectron spectroscopy (XPS). The electrochemical performance of nanofibers was evaluated by cyclic voltammetry and galvanostatic charge-discharge at different current densities. The results showed improved stability at high current densities (344.1 mAh g^{-1} at 5000 mA g^{-1}), more significant charge capacity (599.6 mAh g^{-1} at 500 mA g^{-1}) and higher initial Coulombic efficiency (CE%, 61.1%) for PO samples than NPO.

1. Introduction

After the discovery of the reversible electrochemical intercalation of lithium ions into graphite by Yazami in 1980, lithium-ion batteries (LIBs) making use of graphite-anode materials are being widely used [1, 2]. However, considering the growing energy demand and limited capacity of graphite anode (372 mAh g^{-1}), alternatives have been extensively studied [3].

Cobalt phosphides (Co_xP), being conversion-type anode materials, are considered as promising anode materials owing to their high theoretical capacity (894 mAh g^{-1} for CoP), higher conductivity, considerably low charge/discharge potential and good thermal stability in comparison to insertion-based and alloying-based anode materials [4–6]. Apart from these, Co_xP are of current interest in many research studies recently as other P-based materials provide very low cycling stability [4], while metal nanoparticles formed during the conversion of cobalt phosphides show increased electrochemical activity for the reverse reaction to occur [7]. The main limitation of Co_xP is high first-cycle capacity loss and lower rate performance, originating from high volume expansion and insufficient ionic conductivity. According to Puthusseri et al. the minimum capacity losses can be achieved by compositing with carbon of appropriate content and buffering the volume expansion [5], while reducing the size of materials to the nanoscale level can ensure an increase in the electrolyte contact area and shorten the Li-ion pathways [3, 8]. Designing carbon composite nanofibers by electrospinning with heat treatment allows combining these approaches [9, 10]. Apart from that, the introduction of polyvinylpyrrolidone (PVP) as

*Corresponding author.
E-mail address: ayaulym.belgibayeva@nu.edu.kz

a carbon source results in the high utilization of the anode active materials with cycling [7].

The physical characteristics of electrospun nanofibers after heat treatment, including mechanical properties, chemical stability, crystal structure and composition, are determined to be dependent on the factors such as relative humidity (RH), pre-oxidation and annealing temperature [9, 11, 12]. Thus, electrospun PVP-derived carbon composite nanofibers of Co_xP with different compositions were successfully synthesized varying the heat treatment conditions, and applied as interlayers for lithium-sulfur batteries [13]. This work is focused on the effect of the pre-oxidation step in the synthesis of PVP-derived carbon composite nanofibers of Co_xP, which were electrospun at controlled low RH, on their electrochemical performance as anode materials for LIBs for the first time.

2. Experimental section

2.1 Synthesis of materials

Carbon composite nanofiber mats with cobalt phosphides were synthesized following the earlier report with some modifications [13], general process flow description is given in Fig. 1a. For that, two independent solutions were prepared before mixing. First, 0.43 g of PVP (Sigma-Aldrich, M_w = 1,300,000 g mol^{-1}, dried at 60 °C in a vacuum oven for 24 h) as electrospinning template and carbon source was dissolved in 6 mL of an absolute ethanol (VLSI, 99.5% purity) and put on a magnetic stirrer. Second, 75 µL of phosphoric acid (H_3PO_4) was added onto the 0.32 g of cobalt nitrate hexahydrate (ACS, $Co(NO_3)_2$*$6H_2O$) solute in 2 mL of distilled water. The second cobalt phosphides precursor solution was added onto the carbon precursor solution after it had been totally dissolved. The mixture was magnetically stirred at 600 rpm at standard temperature and pressure (STP) for 15 h. The solution was electrospun with an electrospinning machine (Inovenso) under the following parameters: voltage of 18 kV, tip-to-collector distance of 10 cm, flow rate of 1 mL h^{-1}, making use of a drum-type collector (Fig. 1b). The relative humidity (RH) was adjusted to 25% using a dehumidifier attached chamber. The electrospun nanofibers were dried at 150 °C for 15 h in air after which part of the sample was pre-oxidized at 280 °C for 1 h with a heating rate of 5 °C min^{-1} in air in a muffle furnace (Nabertherm LT 9/13), and the second part was left non-pre-oxidized. Next, both pre-oxidized and non-pre-oxidized samples were heat treated at 700 °C in Ar + H_2 (4%) atmosphere for 1 h with a heating rate of 5 °C min^{-1} in a tube furnace (Across International), and denoted as PO and NPO, respectively. The yield and digital images are shown in Fig. 1c.

2.2 Physical characterizations

Thermogravimetric analysis (TGA) was conducted using Simultaneous Thermal Analyzer

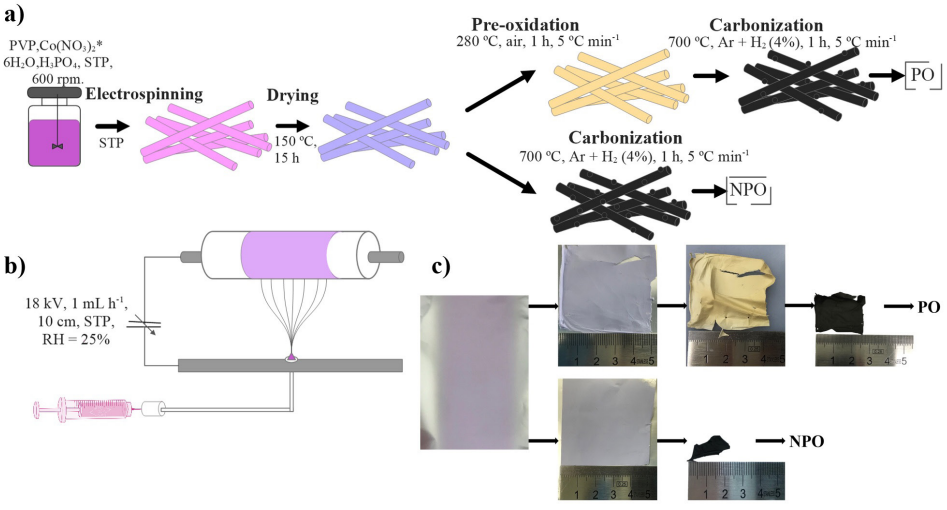

Fig. 1. (a) Synthesis scheme of PVP-derived carbon composite nanofibers of cobalt phosphides, (b) schematic illustration of the electrospinning process, (c) digital images of the fiber mats corresponding to each step in Fig. (a).

(STA) 6000. Molecular structure of nanofibers was obtained from Fourier Transform Infrared (FTIR) Analysis using Nicolet iS10 FT-IR Spectrometer. X-ray Diffraction (XRD) analysis was performed using Miniflex (Rigaku). Raman spectra (532 nm excitation wavelength, 1% of the initial power (15 mW) and 10 s of accumulation time) were recorded using Raman Spectroscopy & AFM Combined System – LabRAM (Horiba). X-ray photoelectron spectra (XPS) were studied using X-ray Photoelectron Spectrometer – NEXSA (Thermo Scientific). The surface of samples was etched for 30 s prior to XPS measurement to reduce the surface oxidation layer. The carbon content of samples was analyzed by CHNS – MicroCube, Elementar. The morphology observations of nanofibers were carried out by Scanning Electron Microscope Crossbeam 540 (SEM, Zeiss).

2.3 Electrochemical characterizations

The electrochemical performance was checked using CR 2032 coin-type cells assembled in a glove box filled with Ar gas of 99.9995% purity. The cells contained Co_xP/C composite nanofibers as free-standing anodes, polypropylene separators, ~50 μL of electrolyte solution consisting of 1 M $LiPF_6$ in the mixture of ethylene carbonate, diethyl carbonate, ethyl methyl carbonate (EC:DEC:EMC) solvents in 1:1:1 vol. ratio, and Li chips as reference electrodes. To check the electrochemical properties of coin-type cells where Co_xP/C nanofibers with a mass-loading of about 0.8–1.2 mg cm^{-2} were used, they were tested through Neware BTS4000 multi-channel battery tester in a potential range of 0.01–3.0 V vs. Li/Li^+ at a current density of 100 mA g^{-1}. The current densities were calculated based on the mass of composite, while capacities were calculated based on the mass of pure Co_xP. Cyclic voltammetry (CV) was conducted in the same potential range at a scan rate of 0.1 mV s^{-1} on a Biologic potentiostat/galvanostat.

3. Results and discussion

3.1 Physical properties of electrospun polyvinylpyrrolidone-derived carbon composites of cobalt phosphide

First, TGA results checking decomposition behavior of nanofibers after drying and pre-oxidation are shown in Fig. 2a. According to that, slight weight loss (2–3 wt%) is observed at around 100 °C corresponding to adsorbed water [14, 15]. Next, weight loss of approximately 7–8 wt% in the case of a dried sample happens at 180–350 °C which probably corresponds to elimination of crystal water (from $Co_3(PO_4)_2$*xH_2O formed after electrospinning) and desorption of hydroxyl group of PVP [16]. At the same time, no change is seen up to 300 °C for pre-oxidized samples due to structural stabilization by prior heat treatment. The major weight loss for dried and pre-oxidized samples up to 450 °C is considered to be thermal decomposition and carbonization of PVP [16–18], further weight loss is caused by the carbothermal reduction of cobalt phosphate. The change in the thermal decomposition behavior of samples after the pre-oxidation step indicates possible differences in the composition and carbon content after the high-temperature annealing. Figure 2b shows FTIR transmittance spectra identifying possible molecular structure of dried, pre-oxidized, NPO and PO samples. The main peaks at 1660, 1440, 1270, 1060, and 660 cm^{-1} corresponding to functional groups of PVP in the dried sample slightly change after the pre-oxidation and disappear after high-temperature annealing [16, 19]. Additional peaks of –C=C− double bond of aromatic carbon groups appear at 1600−1475 cm^{-1} on the spectra of both NPO and PO samples [9], while peaks at ~1000−1200 cm^{-1} may correspond to different Co- and P-based groups.

The crystal structure of the obtained NPO and PO samples was checked by XRD and shown in Fig. 2c. Both samples contain low-crystalline cobalt phosphides in forms of CoP and Co_2P in the orthorhombic Pnma(62) space group. The NPO sample contains more CoP while the PO sample contains more Co_2P which is consistent with the reported works [13, 20]. The Raman spectra are shown in Fig. 2d, D and G bands of graphitic carbon are indicated accordingly. The G band around 1585 cm^{-1} has clearer intensity than the D band approximately at 1345 cm^{-1}. The former indicates that in both samples of NPO and PO the primary mode of graphene exists with a planar configuration of sp^2 bonded carbon [14]. The D band being a defect band, its low intensity means insignificant number of defects present in the material [21]. The I_G/I_D ratios for NPO and PO are 1.037 and 1.035 respectively.

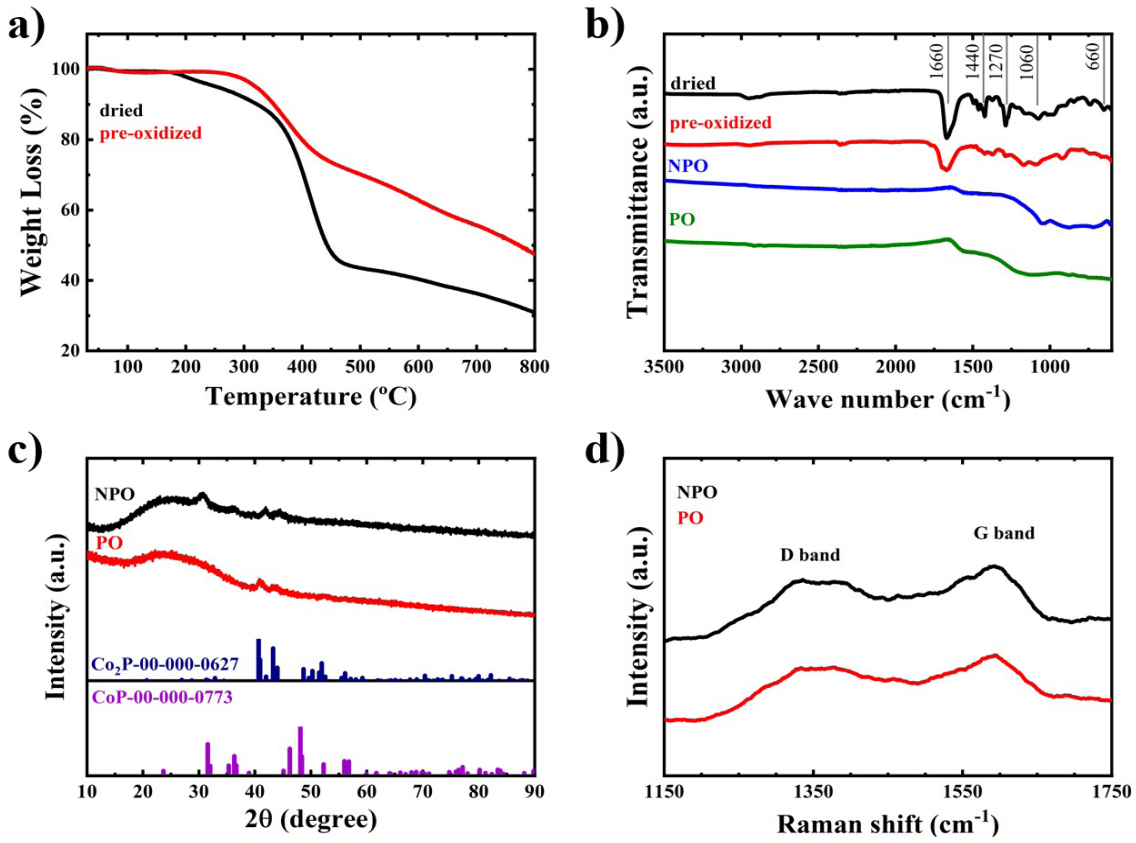

Fig. 2. (a) TGA curves, (b) FTIR transmittance spectra, (c) XRD patterns, and (d) Raman spectra of NPO and PO samples.

The structure of the obtained composites was further studied by XPS and depicted in Fig. 3. Interestingly, despite the absence of the pre-oxidation step, the NPO sample contains more oxygen atoms (Fig. 3a). There is no significant difference in the carbon structure (Fig. 3b) as has been also confirmed from Raman results. On the other hand, Co 2p and P 2p spectra of two samples are clearly different (Fig. 3c and d): peaks located at around 793.5, 778.4, and 129.7 eV indicate formation of Co-P bond of Co_xP in both samples, while other peaks indicate presence of cobalt phosphate ($Co_3(PO_4)_2$ at 797.3, 780.8, 133 eV in PO sample) and cobalt metaphosphate ($Co_2(PO_3)_4$ at 798, 782, and 134.5 eV in NPO sample) [22, 23]. Note, that PO sample contains more oxygen-free Co_xP, which may positively affect its electrochemical performance. Comparing this to previous XRD results, we can confirm the formation of the following composites: $Co_xP/Co_2(PO_3)_4$/C for NPO and $Co_xP/Co_3(PO_4)_2$/C for PO sample.

The content of carbon, determined by CHNS analysis, is equal to 48.5 and 56.9 wt% for NPO and PO samples, respectively (Table). The difference in the composition from the former work [13] can probably be ascribed to the controlled low RH and annealing atmosphere of Ar + H_2 (4%) instead of N_2 + H_2 (3%).

The morphology of NPO and PO samples was observed by SEM analysis and shown in Fig. 4a and b, respectively. Both samples have a nanofibrous structure with similar fiber diameter of around 75–90 nm and clued beads/particles on nanofibers. On the other hand, NPO has curved nanofibers with more particles on the fiber surface, while PO has straight ones with more smooth surface. This difference can potentially affect the electrochemical performance of samples.

Table

Elemental composition of samples determined by CHNS analysis

Sample	C, wt%	H, wt%	N, wt%
NPO	48.50	0.50	3.50
PO	56.90	0.85	3.46

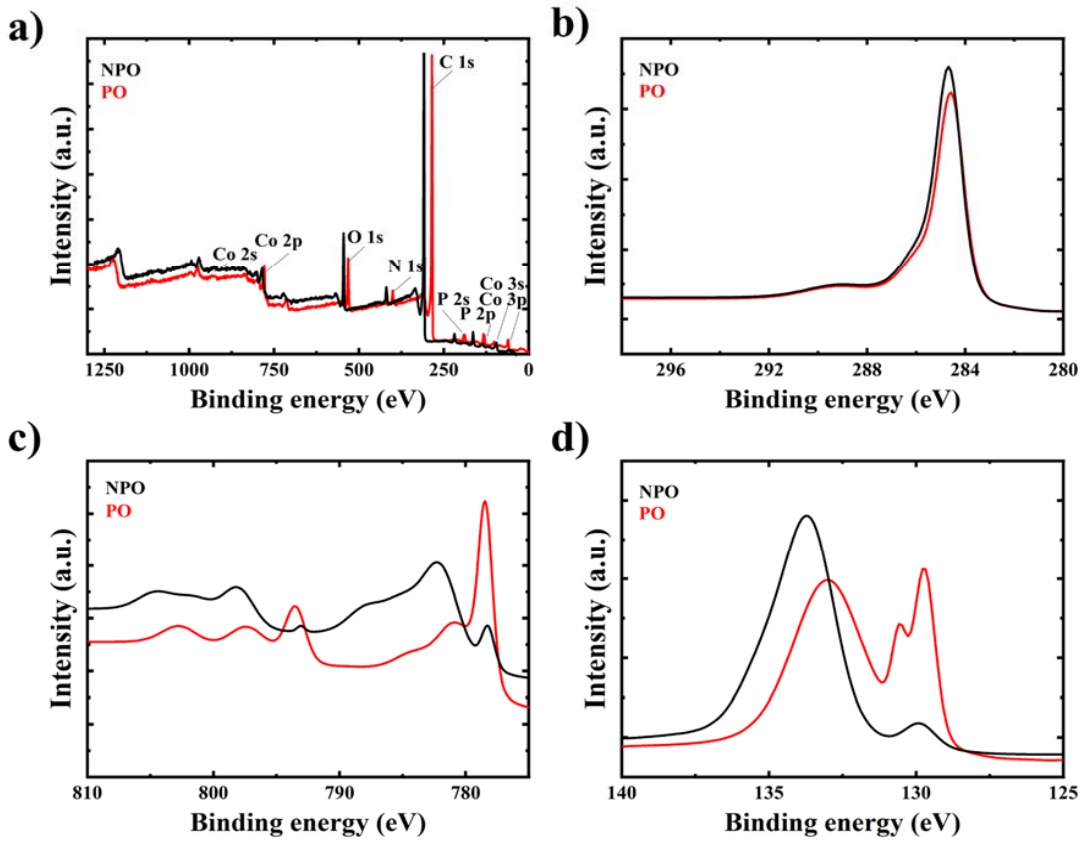

Fig. 3. (a) XPS survey, (b) C 1s, (c) Co 2p, (d) P 2p XPS spectra of the NPO and PO samples.

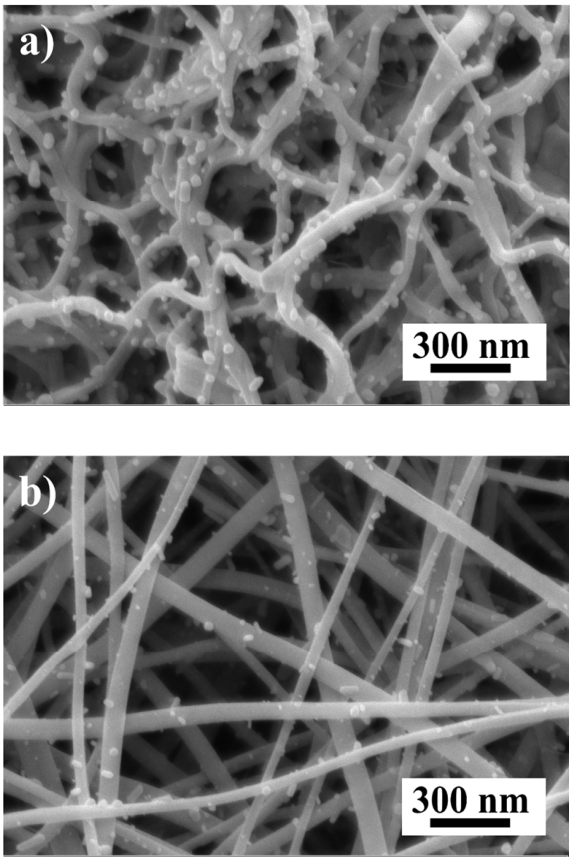

Fig. 4. SEM images of (a) NPO and (b) PO samples.

3.2 Electrochemical properties of electrospun polyvinylpyrrolidone-derived carbon composites of cobalt phosphide

Figure 5a and b show CV curves for NPO and PO samples respectively. In overview, there is a clear difference in their curves due to solid electrolyte interphase (SEI) formation and electrochemical activation in combination with the variations in compositions as it has been revealed by XPS [24]. During the first discharge scan, there are three reduction peaks for NPO (at 1.4, 1.2 and 0.7 V) and a broad peak for PO (at 1.2 V). Peaks at higher potential regions can be ascribed to the lithiation of phosphate components with the formation of Co, $LiPO_3$ (for NPO), Li_3PO_4 (for PO), and SEI layer. Lithiation of phosphide components takes place at lower potential regions with the formation of Co and Li_3P [25–27]. The oxidation peaks observed at 1.3 and 2.6 V for both samples correspond to the Li_3P decomposition and transformation to Co_2P/CoP [25]. As the following cycles repeat the same path, high reversibility of NPO and PO samples can be confirmed. Figure 5c and d illustrate charge-discharge curves at 100 mA g^{-1} for NPO

and PO respectively. Both samples show an incredibly high initial discharge capacities of 1617.5 mAh g^{-1} (NPO) and 1856.2 mAh g^{-1} (PO) while the first charge capacities were 1042.9 mAh g^{-1} and 1150.1 mAh g^{-1} for NPO and PO samples respectively. The PO shows a better cyclic stability with higher capacity retention between the 10th (828.3 mAh g^{-1}) and 50th (798.6 mAh g^{-1}) cycles (96.4% vs. 83.1% for NPO).

According to the rate-capability test results in Fig. 5e, both samples had more than 310 mAh g^{-1} charge capacity even at a high current density of 5000 mA g^{-1}. However, PO regained more capacity when the current density was returned back to 100 mA g^{-1}. Figure 5f shows a cyclability graph with charge capacities at a current density of 500 mA g^{-1} for both NPO and PO including their Coulombic efficiencies (CE%). The initial Coulombic efficiencies were 56.5% and 61.1% for NPO and PO samples respectively. These results are probably linked to irreversible electrolyte decomposition and incomplete backward conversions [5]. Both samples had a similar stability starting from the 15th cycle with CE% of almost 100%. However, PO samples show capacities higher for approximately 50–100 mAh g^{-1} than that of NPO.

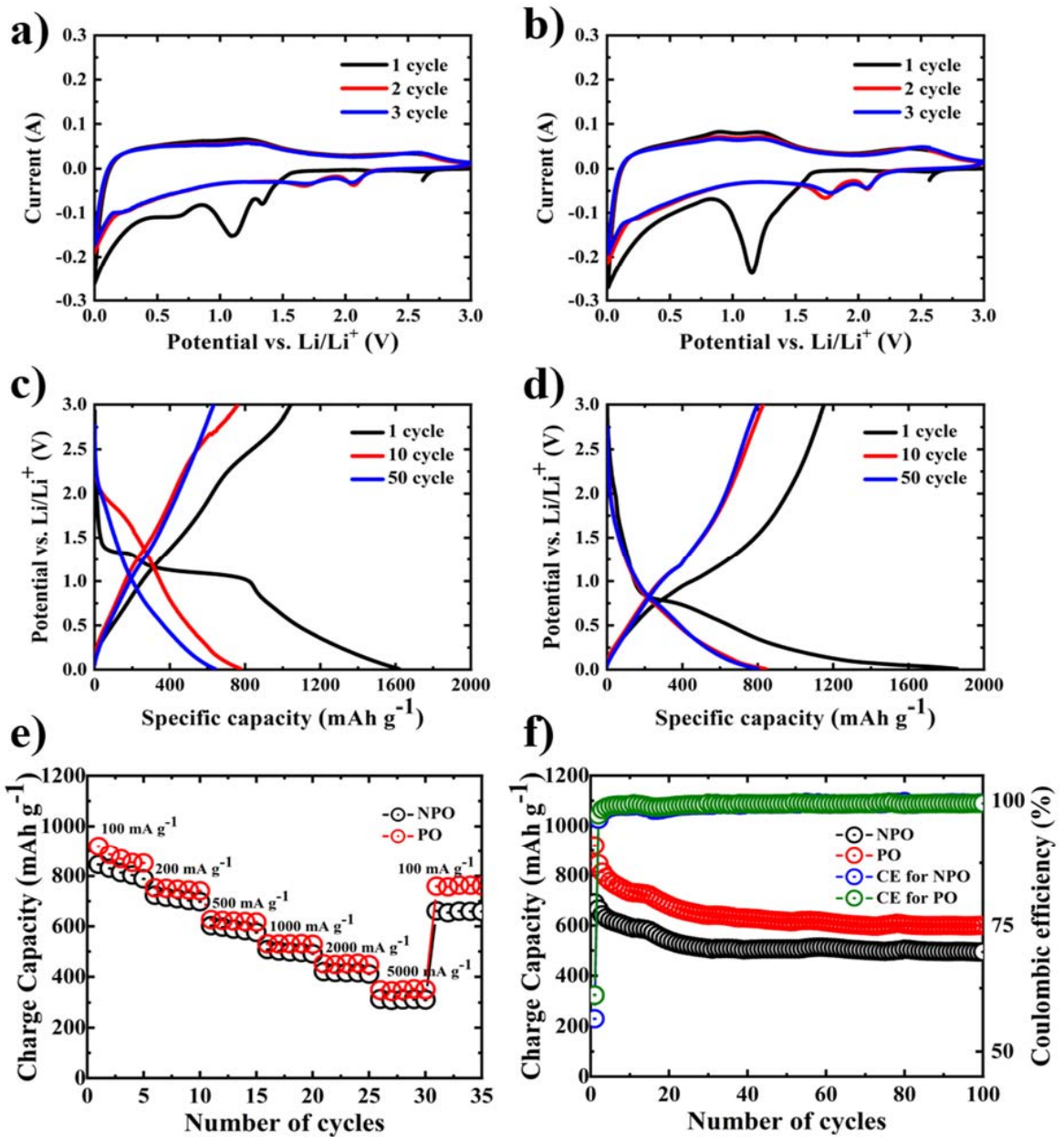

Fig. 5. CV of (a) NPO and (b) PO samples, charge-discharge curves at a current density of 100 mA g^{-1} (c) NPO and (d) PO samples, (e) rate-capability, and (f) cyclability of NPO and PO samples at a current density of 500 mA g^{-1}.

4. Conclusions

In the present work, we investigated the effect of pre-oxidation step on electrospun PVP-derived carbon composites of cobalt phosphide by checking their physical properties and electrochemical performances using them as anode materials in LIBs. According to the provided investigation, the formation of CoP and Co_2P for both NPO and PO samples were proven via XRD analysis while presence of amorphous cobalt metaphosphate for NPO and cobalt phosphate for PO was determined by XPS. Moreover, PO samples showed higher Co_xP and carbon contents and less particles on the surface of PO samples. As a result, the PO samples showed better stability at high current densities (683.1 mAh g^{-1} vs 639.4 mAh g^{-1} at 5000 mA g^{-1}), more significant charge capacity (599.6 mAh g^{-1} vs. 494.4 mAh g^{-1} at 500 mA g^{-1} of current density) and higher initial Coulombic efficiency (61.1% vs. 56.5%) even if they both showed CE% of almost 100% for the following cycles.

Acknowledgments

This research was funded by the project AP13068219 "Development of multifunctional free-standing carbon composite nanofiber mats" from the Ministry of Education and Science of the Republic of Kazakhstan. Authors are grateful to the staff of the Core Facilities of the Nazarbayev University for assistance in conducting the physical characterizations of samples.

References

[1]. R. Yazami, Ph. Touzain, *J. Power Sources* 9 (1983) 365–371. DOI: 10.1016/0378-7753(83)87040-2

[2]. R. Yazami, *J. Power Sources* 97–98 (2001) 33–38. DOI: 10.1016/S0378-7753(01)00737-6

[3]. D. Hao Sim, X. Rui, J. Chen, et al., *RSC Adv.* 2 (2012) 3630–3633. DOI: 10.1039/C2RA20058A

[4]. Y. Yang, Y. Jiang, W. Fu, et al., *Dalton Trans.* 48 (2019) 7778–7785. DOI: 10.1039/C9DT01240K

[5]. D. Puthusseri, M. Wahid, S. Ogale, *ACS Omega* 3 (2018) 4591–4601. DOI: 10.1021/acsomega.8b00188

[6]. D. Yang, J. Zhu, X. Rui, et al., *ACS Appl. Mater. Interfaces* 5 (2013) 1093–1099. DOI: 10.1021/am302877q

[7]. Y. Lu, L. Yu, X.W. (David) Lou, *Chem* 4 (2018) 972–996. DOI: 10.1016/j.chempr.2018.01.003

[8]. X. Rui, H. Tan, D. Sim, et al., *J. Power Sources* 222 (2013) 97–102. DOI: 10.1016/j.jpowsour.2012.08.094

[9]. A. Belgibayeva, I. Taniguchi, *Electrochim. Acta* 328 (2019) 135101. DOI: 10.1016/j.electacta.2019.135101

[10]. L. Li, P. Liu, K. Zhu, et al., *Electrochim. Acta* 235 (2017) 79–87. DOI: 10.1016/j.electacta.2017.03.071

[11]. Y. Zou, Sh. Jiang, X. Hu, et al., *Mater. Today Commun.* 26 (2021) 102069. DOI: 10.1016/j.mtcomm.2021.102069

[12]. M.-R. Ardigo-Besnard, A. Besnard, G.N. Bouala, et al., *Crystals* 12 (2022) 1732. DOI: 10.3390/cryst12121732

[13]. A. Belgibayeva, M. Rakhatkyzy, A. Adi, I. Taniguchi, *ChemElectroChem* 9 (2022) 17. DOI: 10.1002/celc.202200458

[14]. O. Kéri, P. Bárdos, S. Boyadjiev, et al., *J. Therm. Anal. Calorim.* 137 (2019) 1249–1254. DOI: 10.1007/s10973-019-08030-0

[15]. O. Elishav, V. Beilin, O. Rozent, et al., *J. Polym. Sci. B Polym. Phys*. 56 (2018) 248–254. DOI: 10.1002/polb.24538

[16]. W.T. Kim, D.C. Park, W.H. Yang, et al., *Nanomaterials* 11 (2021) 1616. DOI: 10.3390/nano11061616.

[17]. I.M. Szilagyi, E. Santala, M. Heikkilä, et al., *J. Therm. Anal. Calorim.* 105 (2011) 73–81. DOI: 10.1007/s10973-011-1631-5

[18]. N. Trung Hieu, J. Suk, D. Wook Kim, et al., *J. Mater. Chem. A* 2 (2014) 15094–15101. DOI: 10.1039/C4TA02348J

[19]. F. Ji, Y.L. Li, J.M. Feng, et al., *J. Mater. Chem.* 19 (2009) 9063–9067. DOI: 10.1039/b915838c

[20]. Q. Mo, L. He, J. Zeng, Q. Gao, *Nanotechnology* 30 (2019). DOI: 10.1088/1361-6528/AB2993

[21]. Z.A. Mansurov, M. Nazhipkyzy, B.T. Lesbayev, et al., *Eurasian Chem.-Technol. J.* 14 (2012) 19–23. DOI: 10.18321/ectj94

[22]. H.B.M. Sidek, X. Jin, M.S. Islam, S.J. Hwang, *ChemCatChem* 11 (2019) 6099–6104. DOI: 10.1002/cctc.201901386

[23]. Z. Li, Y. Zou, J. Duan, B. Long, *Ionics* 25 (2019) 4625–4635. DOI: 10.1007/s11581-019-03047-9

[24]. I. Kurmanbayeva, A. Mentbayeva, A. Sadykova, et al., *Eurasian Chem.-Technol. J.* 21 (2019) 75–81. DOI: 10.18321/ectj794

[25]. Y. Liu, X. Que, X. Wu, et al., *Mater. Today Chem.* 17 (2020) 100284. DOI: 10.1016/j.mtchem.2020.100284

[26]. H. He, L. Zeng, X. Li, et al., *ACS Appl. Mater. Interfaces* 13 (2021) 34410–34418. DOI: 10.1021/acsami.1c08950

[27]. S. Hao, B. Ouyang, C. Li, et al., *J. Phys. Chem. C* 123 (2019) 8599–8606. DOI: 10.1021/acs.jpcc.8b12494